Title

ENHANCEMENT OF TWO PROTON TRANSFER IN N = 82 NUCLEI. A STUDY OF 1p-, 2p-, AND (2p + 2n)-TRANSFER REACTIONS INDUCED BY l6O ON l40Ce, 142Nd, AND 144Sm NEAR THE COULOMB BARRIER

Authors

Oertzen, Wolfram von
Bohlen, H.G.
Gebauer, B.

Publication Date

1973

Submitted to Nuclear Physics

LBL-1622
Preprint c.1

ENHANCEMENT OF TWO PROTON TRANSFER IN N = 82 NUCLEI. A STUDY OF 1p-, 2p-, AND (2p + 2n)-TRANSFER REACTIONS INDUCED BY ^{16}O ON ^{140}Ce, ^{142}Nd, AND ^{144}Sm NEAR THE COULOMB BARRIER

Wolfram von Oertzen, H. G. Bohlen, and B. Gebauer

January 1973

Prepared for the U.S. Atomic Energy Commission
under Contract W-7405-ENG-48

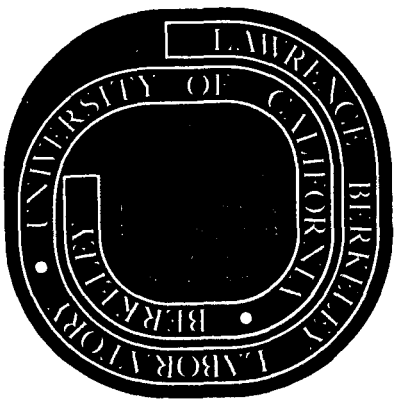

DISCLAIMER

ENHANCEMENT OF TWO PROTON TRANSFER IN N = 82 NUCLEI. A STUDY OF 1p-, 2p-, AND (2p + 2n)-TRANSFER REACTIONS INDUCED BY ^{16}O ON ^{140}Ce, ^{142}Nd, AND ^{144}Sm NEAR THE COULOMB BARRIER[†]

Wolfram von Oertzen

Lawrence Berkeley Laboratory
University of California
Berkeley, California 94720

and

Max Planck Institut für Kernphysik
Heidelberg, West Germany

and

H. G. Bohlen and B. Gebauer

Max Planck Institut für Kernphysik
Heidelberg, West Germany

January 1973

Key Words:

Nuclear Reactions (^{16}O,^{15}N), (^{16}O,^{14}C), (^{16}O,^{12}C) on ^{140}Ce, ^{142}Nd, ^{144}Sm. E = 63-66.5 MeV. Measured $\sigma(\theta)$, $\sigma(E)$; deduced transfer probability. Enriched targets.

[†]Work partly supported by the U.S. Atomic Energy Commission.

Abstract

One-proton, two-proton, and "α-particle" transfer have been studied on nuclei with closed neutron shell N = 82 using ^{16}O beams of 63 MeV to 66.5 MeV incident energy. Transfer probabilities defined in a semiclassical model are derived for the different reaction channels. For this purpose the Q-value and angular dependence of the cross section are discussed. The two-proton transfer to the ground states shows an enhancement by a factor 20-25 compared to other nuclei, showing the effect of the proton pairing in these nuclei (they correspond to equivalent neutron configurations in $^{108,110,112}Sn$). The total transfer probability follows a common trend for all three target nuclei as a function of energy above the Coulomb barrier for the proton and two-proton transfer, respectively, but not for the four nucleon transfer.

1. Introduction

Recently, several studies of single and multinucleon transfer reactions induced by ^{16}O on heavy nuclei have been reported[1-4]). Of particular interest are the two-proton and two-proton + two-neutron (α-particle) transfer reactions, because they can yield new information on proton and neutron pairing interactions. ^{16}O induced reactions on heavier nuclei are characterized by a large value of the Sommerfeld parameter η and therefore show marked characteristics of reactions proceeding under semiclassical conditions[5,6]). The conditions for maximum cross sections are very stringent and lead to very sensitive dependence of the cross section on kinematical factors. The strong dependence of the reaction cross section on Q-value[2,4,7]) necessitates a careful study of the dynamical properties of the heavy ion transfer reaction. DWBA calculations neglecting recoil terms have been quite successful in explaining general features of single nucleon transfer reactions[2]) although certain discreapancies with experimental data can only be removed by including recoil terms in the DWBA[8]) or by applying complete finite range calculations[9,10]).

The present study of transfer reactions was undertaken on nuclei with a closed neutron shell (N = 82) and open proton shell corresponding to the analogous situation for neutrons in the Tin isotopes (where the Z = 50 closed proton shell combines with an open neutron shell). The nuclei chosen are spherical and ^{144}Sm (Z = 62) corresponds to ^{112}Sn, ^{142}Nd (Z = 60) to ^{110}Sn and ^{140}Ce (Z = 58) to ^{108}Sn. The Q-values for the one-proton, two-proton and four nucleon transfer are negative. The incident energies were chosen in such a way that the favored Q-values were in the vicinity of the Q-values for the ground state transitions. The incident energies were thus only a few MeV above the

Coulomb barrier, a fact which made it necessary to observe the reaction products at large angles (150°-170° Lab). Nevertheless, in the four nucleon transfer reactions the ground state transitions could not be measured in all cases, because of a considerable mismatch in Q-value.

A pairing force acting between the protons should manifest itself in proton-superfluid states in the nuclei ^{142}Nd to ^{146}Gd. If the (^{16}O,^{14}C) reaction proceeds predominantly by the transfer of a proton pair in an S = 0, T = 1 state, the two-proton transfer should be enhanced by an equivalent factor as observed in (t,p) reactions on Tin-isotopes.

2. Experimental Technique and Results

The experiments were performed using the ^{16}O beam of the Heidelberg MP Tandem. The targets ranged in thickness from 100 $\mu g/cm^2$ to 300 $\mu g/cm^2$ and were deposited on ^{12}C backings. Due to the fact that all measurements were performed at angles between 150° Lab and 170° Lab no contimanation lines from the backing could interfere with the relevant spectra of ^{12}C, ^{14}C, and ^{15}N particles. All targets were made from material enriched to more than 98%.

The particles were identified using ΔE - E telescopes. The ΔE counters were of thickness between 18μ to 25μ. The heaviest particles, ^{16}O and ^{15}N left up to 3/4 of their total energy in the ΔE counter. The ΔE and E pulses were added at high level and given (via biased amplifiers) onto two-dimensional analyzers (128 × 128). Up to three ΔE - E telescopes were used simultaneously using two ND 128 × 128 analyzers and an online computer for the storage of the data. The separation of ^{12}C and ^{14}C was usually complete with ΔE counters with a thickness larger 20μ.

The energy resolution was typically 400 to 500 keV. The target thickness contributed the largest part to the energy spread due to the fact that for the difference in energy loss between the incoming and outgoing particles the target thickness enters twice for reactions observed at backward angles. At angles of approximately 150° Lab the outgoing particles pass through the target material at an angle to the incident beam (target being at a right angle to the beam direction) and are submitted to a longer path through the target material than the incoming ^{16}O ions. The difference in total energy loss between ^{16}O and ^{14}C (or ^{16}O) ions considering reactions taking place on the front or backside of the target can be rather large. The ^{14}C,^{12}C spectra often show a better resolution

than the elastically scattered ^{16}O due to a smaller difference in energy loss between ^{14}C and ^{16}O at angles of 150°.

The ^{16}O and ^{15}N spectra were processed with an automatic computer program which fits polynomy to the different element lines in the two dimensional matrix of $\Delta E + E$ and ΔE. The ^{14}C and ^{12}C were separated by hand from printout on paper. In some cases, especially at the higher energies above Coulomb barrier, intensities between the ^{12}C and ^{14}C lines were observed which could be assigned to ^{13}C. In view of the fact that their separation was usually not unique and their intensity was usually less than 5% of the total yield of either ^{12}C or ^{14}C no attempts were made to deduce ^{13}C yields. The ^{12}C and ^{14}C yields given in the next section both contain parts of the ^{13}C yield if any was present.

The same applies to the ^{14}N yield, whose identification was not unique. The ^{15}N yield thus may contain ~ 5% to max. 10% of ^{14}N.

During all the measurements the elastic scattering was recorded simultaneously with the total nitrogen and carbon spectra. Thus the normalization of the data was made with respect to the elastic scattering. Detoriation of the target, if it occurred, therefore could not interfere with the normalization of the data.

For all three targets ^{140}Ce, ^{142}Nd, and ^{144}Sm several angles, usually four (150°, 155°, 160°, 165°, sometimes 170°, Lab) were measured at each energy. Spectra of ^{15}N, ^{14}C, and ^{12}C for each target are shown in fig. 1. The ground state Q-values for the two-proton transfer vary from target to target and a corresponding change in the strength of the ground state transitions in the $(^{16}O,^{14}C)$ reaction is observed reflecting the strong Q-value dependence of the reactions (see next section). The Q-values for the one-proton and α-particle

transfer vary less strongly. For the (^{16}O,^{12}C) reactions only extremely weak transitions to the ground states could be observed, the reaction proceeds mainly to regions of approximately 8 MeV excitation in the final nucleus due to the rather negative optimum Q-values. Figure 2 shows in a logarithmic scale two (^{16}O,^{14}C) and (^{16}O,^{12}C) spectra for the ^{140}Ce target, the ^{14}C spectrum being shifted by 5 channels. The similarity between the two spectra is rather evident. Whereas the Q-values for the ground state transition are rather similar (9.2 MeV for ^{12}C and 9.8 MeV for ^{14}C) the reactions proceed mainly to different final excitations possibly due to a corresponding difference in optimum Q-value, (see section 4.3) or due to differences in level densities in the final nucleus.

Figure 3 shows the same spectra in a linear scale. There are definite peaks in the (^{16}O,^{12}C) spectrum at high excitation. Similar peaks which separate well from a general curve and which can be identified at several incident energies are observed with the other targets too (fig. 4). In the reaction $^{142}Nd(^{16}O,^{12}C)^{146}Sm$ peaks are observed at 6-8 MeV excitation in the final nucleus (fig. 5) where the level density is of order 100-1000/MeV. The spectra shown in fig. 5 were measured with the same experimental calibration. The peak intensity of the spectrum thus remains at the same final laboratory energy for the three energies (63 MeV, 64 MeV, and 65 MeV) at a given angle. The optimum Q-value thus becomes more negative with increasing incident energy by approximately 1 MeV (see also next section).

At the energies chosen the intensity as a function of scattering angle has its maximum at approximately 160° Lab ($\approx$ 163° cm). Figure 6 shows as an example the total yield (divided by elastic yield) for ^{15}N, ^{14}C, and ^{12}C nuclei in the reactions induced by ^{16}O on ^{140}Ce at 64 MeV as a function of scattering angle.

3. Analysis of the Data

For the analysis of the data the strong dependence of the cross section on Q-value, scattering angle and angular momentum has to be discussed. Different transfer reactions on a variety of nuclei can then be reduced to corresponding values at the same kinematical condition. The reduced cross section is then given by:

$$\bar{\sigma}_{exp}(Q_o,\theta_o) = \sigma_{exp}(Q,\theta) \cdot \frac{\sigma_c(Q_o,\theta_o)}{\sigma_c(Q,\theta)} \quad , \; \sigma_c(Q,\theta) \text{ - calculated cross sections}$$

In semiclassical conditions the reduced experimental cross section can be replaced by an appropriate semiclassical transfer probability as discussed in the following. The grazing angle θ_o, which is different for different targets and incident energies can be replaced by a distance parameter d_o determined by the relation:

$$R = d_o(A_1^{1/3} + A_2^{1/3})$$

and relation (1) between minimum distance and scattering angle given below. The transfer probability $P_{tr}(d_o)$ deduced from $\bar{\sigma}_{exp}(Q_o,\theta_o)$ is the function, which does not contain any more kinematical factors and can be compared for different nuclei.

3.1. SEMICLASSICAL CONSIDERATIONS

Reactions proceeding at conditions with large values of the Sommerfeld parameter η, $\eta = \frac{Z_1 Z_2 e^2}{\hbar v}$, can be described by semiclassical models[5,6]. This fact is connected with the circumstance that the deBroglie-Wavelength $\lambda\!\!\!^{-}$ of the

relative motion is small compared to typical distances R, the distance of closed approach in a scattering orbit. The distance is for given scattering angle θ, and wave numbers k, given by

$$R = \frac{\eta}{k}\left(1 + \frac{1}{\sin\,\theta/2}\right) = \eta\cdot\lambda\left(1 + \frac{1}{\sin\,\theta/2}\right) = \frac{Z_1 Z_2 e^2}{2E_{CM}}\left(1 + \frac{1}{\sin\,\theta/2}\right) \tag{1}$$

Under semiclassical conditions the total transfer cross section can be factorized into a scattering probability $|f_{sc}(\theta)|^2$ and transfer probability $P_{tr}(\theta)$

$$\frac{d\sigma}{d\Omega}(\theta) = |f_{sc}(\theta)|^2 \cdot P_{tr}(\theta) \tag{2}$$

The scattering probability is determined by a classical orbit and can be described rather satisfactory by the Rutherford scattering σ_R multiplied with an adequate absorption function $F_{abs}(\theta)$ (ref. [4])). The transfer probability strongly depends on the differences between the initial and final orbit (and thus on Q-value) described by a function F(Q). Thus we obtain

$$\frac{d\sigma}{d\Omega}(\theta) = \sigma_R(\theta) \cdot F(Q) \cdot F_{abs}(\theta); \qquad F_{abs}(\theta) = 1 - P_{abs}(\theta) \tag{3}$$

and we have for elastic scattering with absorption

$$\frac{\sigma}{\sigma_R}(\theta) = 1 - P_{abs}(\theta) \tag{4}$$

The probability of absorption $P_{abs}(\theta)$ can be described satisfactorily for a large variety of nuclei as suggested by Christensen *et al.*[4]) using the function

$$P_{abs}(R) = \begin{cases} 0; \; R \geqslant R_o \\ 1 - \exp\left(\frac{R - R_o}{\Delta}\right); \; R < R_o \end{cases} \tag{5}$$

The relation between scattering angle θ and minimum distance R can be taken as relation (1) — neglecting the real potential. The real potential usually has little influence for distances larger R_o, the interaction radius. R_o being determined by a parameter r_o

$$R_o = r_o(A_1^{1/3} + A_2^{1/3}) \tag{6}$$

The value $r_o = 1.68$ fm was found to describe the elastic scattering data rather satisfactory, and with $\Delta \cong .55$ fm.

The concept of classical orbits implies specific conditions on changes of the parameters for the final scattering state. Matching of the orbits of the incoming and outgoing channel at the minimum distance leads to the classical condition for maximum cross section as suggested by Buttle and Goldfarb[5])

$$\frac{\eta_i}{k_i}\left(1 + \frac{1}{\sin\theta_{i/2}}\right) = \frac{\eta_f}{k_f}\left(1 + \frac{1}{\sin\theta_{f/2}}\right) \tag{7}$$

An optimum Q-value is thus obtained from expression (7) assuming $\theta_i = \theta_f$

$$Q_{opt} = E^i_{CM}\,\frac{Z_3Z_4 - Z_1Z_2}{Z_1Z_2}\;;\; Q_{opt}\ 1 \tag{8}$$

The angular momentum transfer is then strictly determined by the relations

$$\ell_i = \frac{\eta_i}{2}\cot\left(\frac{\theta_i}{2}\right);\; \ell_i - \ell_f = (\eta_i - \eta_f)\tfrac{1}{2}\,\mathrm{ctg}\;\theta/2 \tag{9}$$

Usually transfer reactions proceed not at the optimum Q-values. The cross section is smaller in non-optimum conditions and depends via the function F(Q) approximately by a Gaussian function[6]) on the parameter ΔD; $(R_i - R_f) = \Delta D$, α-decay constant of the bound state.

$$F(Q) \sim \exp\left(-\frac{|\Delta D|^2}{\alpha \cdot R \cdot \lambda^2}\right) \tag{10}$$

An alternative description for the optimum Q-value is suggested by fig. 5. Given a certain charge product Z_3Z_4, a scattering angle θ_f (where the counters are placed) and a minimum distance determined by the strong absorption radius defined in expression (6), eq. (1) defines a fixed final energy E^f_{cm} which can fulfill eq. (1). The "optimum" Q-value for this angle will be then

$$Q_{opt} = E^f_{CM} - E^i_{CM} = \frac{Z_3Z_4}{2R_o}\left(1 + \frac{1}{\sin\theta/2}\right) - E^i_{CM} \; ; \qquad Q_{opt\ 2} \; . \tag{11}$$

Equation (11) gives in the present case a change for Q_{opt} by -.9 MeV per 1 MeV change in E^i_{Lab}. Equation (8) for the optimum Q-value gives only a change of Q_{opt} of .25 MeV per 1 MeV change in incident energy. (Q_{opt} here is the percentage change in charge times incident energy; and $(Z_1Z_2 - Z_3Z_4)/Z_1Z_2$ is 25%). $Q_{opt\ 2}$ from expression (11) depends on the choice of R_o, the interaction radius (which may be different for different transfer reactions, see also section 4.3).

The experimental result in the present case seems to be consistent with eq. (11) as shown in figs. 5a and 5b and Table 1, where different semiclassical calculations of Q_{opt} and Q_{exp} are compared. Similarly, the variation of Q_{opt} with incident energy observed in (^{16}O,^{12}C) reactions on ^{90}Zr and ^{172}Yb (ref. [11])) was found to be inconsistent with expression (8). The results of ref. [11]) are, however, well

described by eq. (11). We may conclude that at energies above Coulomb barrier and scattering angles $\theta \geq \theta_o$ the position of the Q-value window is mainly determined by the existence of an absorptive radius R_o; Q_{opt} is then given by relation (11). At energies below the Coulomb barrier or at angles $\theta < \theta_o$ the matching condition for the scattering orbits determines Q_{opt}, which is then determined by relation (8). Inclusion of a recoil factor as discussed in refs. [5,12,13]) gives slightly more negative values for $Q_{opt\ 1}$. $Q_{opt\ 2}$ values given in Table 1 are probably to high due to the value for $r_o = 1.68$ fm. We also deduce from the table that DI = R^i_{min} is usually smaller than the interaction distance R_o (which implies that $\theta > \theta_o$) and that the relevant optimum Q-value will be $Q_{opt\ 2}$. ($r_o = 1.63$ fm gives values for $Q_{opt\ 2}(^{14}C)$ which are 1.5 MeV smaller.) If the reaction proceeds to the optimum Q-value the scattering cross sections (or amplitudes) become the same in the initial and final channel because $\frac{\eta}{k}$ is the same and

$$\sigma_R \sim \frac{\eta^2}{k^2} \tag{12}$$

If the total radii change not too much in the reaction we have also $(\sigma/\sigma_R)_i = (\sigma/\sigma_R)_f$, i.e., the same degree of absorption is observed in the initial and final channel (see also fig. 10) for optimum Q-values.

In cases of Q-value mismatch (however, not too large mismatch, because semiclassical models would fail in these cases) the differential cross section can be written as[4]); $\bar{\sigma}_R$ is an average elastic Coulomb scattering cross section

$$\frac{d\sigma}{d\Omega}(\theta) = \sqrt{(\sigma/\sigma_R)_i (\sigma/\sigma_R)_f}\ \bar{\sigma}_R \cdot P_{tr}(\theta) \cdot F(Q) \tag{13}$$

Using this equation, $P_{tr}(\theta)$ or preferably $P_{tr}(d_o)$ can be deduced from the data, d_o is the radius parameter connected with the minimum distance R in an average orbit and through relation (1) related to the scattering angle θ. $P_{tr}(d_o)$ is then the quantity which can be compared for different targets.

3.2. DWBA CALCULATIONS

Using the no-recoil approximation and the procedure of Buttle and Goldfarb[5]) the DWBA transition amplitude can be calculated[7]) using standard DWBA codes.

In the present case we used the code DWUCK[14]) to calculate the Q-value dependence of the differential cross section for the different reactions. It was assumed that the two protons are transferred in an S = 0, and T = 1 state. The bound state in the final channel for the present target nuclei has as quantum number 5S for the relative motion of the center of mass of the two protons (the oscillator shell for the single nucleons is 3S, 2d, and 1g). The optical model parameters were chosen to be those of ref. [4]), and were derived from the elastic scattering of ^{16}O on nuclei in the mass range 48 to 90. The parameters gave equally good fits to the elastic scattering of ^{16}O on ^{208}Pb [3]).

Figure 7 shows as an example the results of the calculations for the $^{140}Ce(^{16}O,^{14}C)^{142}Nd$ reaction. The dotted curves were obtained using the same final bound state for the various Q-values. These curves illustrate the effect of the mismatch of the scattering waves in the incident and final channel and the effect of absorption which decreases the cross section drastically if in one of the channels σ/σ_R is small and much different from the other channel as discussed in the previous section and described by eq. (13).

The inclusion of the proper variation of the binding energy of the bound state yields the full curves in fig. 7. Different angular momentum transfers

peak at the same Q-value. There is a variation of the optimum Q-value (point of maximum cross section) with incident energy which amounts to .9 MeV per 1 MeV change in incident energy. This prediction agrees rather well with the experimental observation, and with the second semiclassical calculation of $Q_{opt\ 2}$ in section 4.1. Higher angular momentum transfer gives larger cross sections for all Q-values. Specifically, transfer of large L-values can bridge large gaps between scattering waves at more negative Q-values. The shape of the spectra of ^{12}C and ^{14}C nuclei is thus most probably determined by higher angular momentum transfers at higher excitation energy as illustrated in fig. 8.

The inclusion of recoil terms is expected to shift the position of the maximum to more negative Q-values[5,12,13]. A rough estimate based on the idea that the incoming ^{14}C particle in the ^{16}O projectile is matched with its orbit to the outgoing ^{14}C particle gives a shift of 1.5 MeV for the (^{16}O,^{14}C) reactions.

Calculations as shown in fig. 7 have been performed for all target nuclei. For the reactions on ^{142}Nd and ^{140}Ce a correction factor was then deduced from these curves to give the cross section and transfer probability at the optimum Q-value. The correction factors are defined by $\frac{\sigma(Q_{opt})}{\sigma(Q_{gs})} = F$ at a given angle. For the ^{144}Sm no correction was necessary because the ground state Q-value (13.7 MeV) coincides rather well with the optimum Q-value ($\sim$ -14 MeV). Table 2 gives the experimental yield for the ground state transitions divided by the elastic yield, the correction factors applied, d_o, and the final transition probabilities $P_{tr}(d_o)$. The correction factors obtained using the semiclassical description, F_2(SC) - in table, are in very good agreement with those obtained from the DWBA curves, F_1 (DWBA).

4. Discussion of the Results

For each target the energy integrated yield divided by the elastic yield is shown at 150° for the ^{15}N, ^{14}C, and ^{12}C in fig. 9 as a function of incident energy above Coulomb barrier which are shown by the same symbols for each target. The scale for the energy above Coulomb barrier was changed by -6 MeV, because deviations from the classically determined Coulomb barrier (r_o = 1.44 fm) are usually observed at approximately 10% smaller energy (see also fig. 10). There is a steep rise of the cross section as a function of incident energy, which is well reproduced in its trend by DWBA calculations with final channels corresponding to the optimum Q-value.

There are usually only a few single particle states which are populated in the one proton transfer reaction (see also fig. 11). The summed single particle strength (folded with the Q-value window) is the same in the three nuclei, because the Fermi surface is spread over many shell model states. Therefore, it can be anticipated that the measured points shown in fig. 9 fall on a common curve for ^{15}N nuclei.

Somewhat less expected is the fact that the total yield for ^{14}C nuclei also follows a common curve. As can be seen from fig. 1 and as suggested by the elastic scattering cross sections in fig. 10 and eq. (8), the ground state transition is only a minor proportion of the total yield for the ^{140}Ce target, is approximately 20%-50% of the total yield for ^{142}Nd and is 80%-90% of the total yield for the ^{144}Sm target. Corresponding to the change in the ground state Q-value a very different proportion of the total transition strength goes to higher excitations in the final nucleus filling the Q-value window with the

same total transition probability. Whether this fact is manifestation of a sum rule or of a constant total strength within the kinematical window is not clear.

The yield for the four nucleon transfer follows different curves for each target. ^{144}Sm gives the largest yield.

The discussion of the enhancement factors for two-proton transfer in the semiclassical model is rather simple for two reasons. First, the scattering process can be discussed independently from the transfer process. Second, if one uses the expansion of the two-proton wave function in terms of Hankel functions and applies the Buttle-Goldfarb method[5]) for the form factor an approximate separation of spectroscopic amplitude and form factor can be obtained because the radial dependence of the form factor will be given by the same Hankel function for all two-proton configurations ($h_\ell^{(1)}(i\alpha r)$, with $\ell = 0$, angular momentum transfer and α-decay constant in the assymptotic region). In the present analysis the comparison of the transfer probabilities at Q_{opt} (fig. 12) corresponds to a comparison of the spectroscopic amplitudes with form factors with the same ℓ but somewhat different decay constants α.

4.1. PROTON TRANSFER

The three target nuclei studied here have 8 to 12 protons more than the closed shell at Z = 50. The $2d_{5/2}$ shell would reach to Z = 56. Proton transfer reactions studied by (^3He,d) reactions[15,16]) showed appreciable $2d_{5/2}$ strength in $^{145}Eu_{63}$. Figure 11 shows the ^{15}N spectra obtained in the present experiments with the localizations and spectroscopic factors for the single particle levels indicated (as obtained in refs. [15,16]). The proton orbits $2d_{5/2}$, $g_{7/2}$, $3S_{1/2}$,

$h_{11/2}$, $2d_{3/2}$ are all active in the nuclei ^{140}Ce to ^{144}Sm. The Fermi surface thus is spread out very strongly due to the proton pairing interaction. (A spectroscopic factor of 0.3 is still measured for $2d_{5/2}$ in ^{145}Eu, which is 6 protons away from the usual closure of the $2d_{5/2}$ subshell at Z = 56.)

Due to the strong localization of the heavy ion reaction to the nuclear surface $3S_{1/2}$ levels are excited the strongest, because they have the largest number of nodes in the bound state wave function. The spectra also show indications of the j-dependence observed by Kovar et al.[3]). The proton being transferred from ^{16}O in a j-lower ($P_{1/2}$) orbit the maximum angular momentum transfer and thus the larger cross section is observed for the j-upper states ($2d_{5/2}$) in the final nucleus.

4.2. TWO-PROTON TRANSFER

Two-proton transfer spectra have been shown in figs. 1 to 4. For a discussion of a possible enhancement of the two-proton transfer, two methods are possible. The first consists in a comparison of the transfer probability defined in section 3.1 for one-proton with that for two-protons; the second consists in a comparison of two-proton transfer probabilities in the N = 82 nuclei with those on other target nuclei (data are available for masses A = 40-90 in refs. [1,2,4]).

The ratio between transition probabilities for 1p-transfer (summed over all single-particle states) and two-proton transfer is at 150° (for ^{144}Sm).

$$\frac{P_{1p}}{P_{2p}} \cong 5, \text{ (see fig. 9).}$$

For ^{144}Sm the ^{15}N spectrum contains mainly two levels and the ^{14}C spectrum consists to 90% of the ground state transition. The transfer probability

for single nucleon transfer is proportional to $P_{1p} \sim 1/A$ (A-target mass), the transfer probability for two-nucleon transfer is proportional to $\sim 1/A^2$; $P_{2p} \sim 1/A^2 \cdot EF$. The enhancement factor EF will be larger unity if the two nucleons are transferred as a pair. From the result $P_{1p}/P_{2p} = 5$ we obtain $EF = A^2/A \times 5 \cong 27$. Alternatively EF can be deduced from fig. 9. For ^{144}Sm we have $(P_{1p})^2 = 5.10^{-4}$ and $P_{2p} \cong 1.10^{-2}$; defining EF by $P_{2p} = (P_{1p})^2 \cdot EF$, this gives $EF \approx 20$. In the present estimation it is assumed that the Q-value is optimum for the single-proton and two-proton transfer. This assumption is actually well fulfilled as can be seen from Table 1.

Using the DWBA calculations illustrated in fig. 7 to correct the experimentally measured transition probabilities (yield/elastic yield) to the transition probability at Q_{opt} we obtain the values for $P_{tr}(d_o)$ shown in fig. 12. Also given in fig. 12 are transition probabilities derived using eq. (13) for (^{16}O,^{14}C) reactions ^{54}Fe, ^{64}Ni, ^{88}Sr given in ref. [4]) and transformed to the d_o scale of fig. 12. Different incident energies at the same angle or different angles at a given energy give $P_{tr}(d_o)$ at different values of d_o. For the nucleus ^{140}Ce the strongest mismatch occurs and the correction factors become rather sensitive to details of the calculations. The inclusion of recoil in DWBA gives for ^{140}Ce values for $P_{tr}(d_o)$ which are by a factor 2 larger, which brings its value near to the value of the other target nuclei.

Figure 12 exhibits a pronounced difference between $P_{tr}(d_o)$ for the N = 82 nuclei and nuclei in the fp-shell (^{54}Fe,^{64}Ni). The two-proton transfer is enhanced by a factor 20-30 in the N = 82 nuclei compared to ^{54}Fe and ^{64}Ni. This value is consistent with the value obtained before from the comparison with single-nuclear transfer. The different slopes of $P_{tr}(d_o)$ are connected with

differences in the binding energy of the proton pair, the Q-values for the N = 82 nuclei being more negative and binding energies being larger.

The two-proton transfer on ^{88}Sr (and the adjacent nuclei, see ref. [4]) seems to be enhanced too. ^{88}Sr has a closed neutron shell (N = 50) and an open proton shell, however, with smaller j-values involved in the individual shell model orbits. The enhancement factor is smaller and is approximately a factor of 5 relative to ^{54}Fe and ^{64}Ni.

We conclude that the two-proton transfer in the reactions (^{16}O,^{14}C) is enhanced in regions where proton pairing is expected to lead to a large spread of the Fermi surface. In a microscopic description the two-particle transfer consist of a coherent sum over all active shells, and the enhancement of the (^{16}O,^{14}C) reaction on the N = 82 nuclei is the result of the coherent action of the $d_{5/2}$, $3S_{1/2}$, $g_{7/2}$, $h_{11/2}$, and $d_{3/2}$ shells. The corresponding enhancement is observed in (t,p) reaction on Tin isotopes, where the same shells are active in two-neutron transfer.

In the reaction $^{118}Sn(t,p)^{120}Sn$ an enhancement factor (defined in a slightly different way) of ca.35 was deduced[18]).

4.3. FOUR-PARTICLE TRANSFER

Spectra of "α-particle" transfer have been shown in figs. 1-5. Due to the less negative Q-values for the four-particle transfer the Q-value window leads mainly to transitions with 4-8 MeV excitation in the final nucleus. In addition the intensity in the spectra of ^{12}C has its maximum at approximately 3 MeV more negative Q-value compared to the ^{14}C spectra (figs. 1-5). An explanation of this circumstance could be found in the fact that the interaction radius is smaller for the two-proton transfer reaction compared to α-particle

transfer. Actually, for all target nuclei of the present experiment, α-particle emitting nuclei are formed in the (^{16}O,^{12}C) reaction (i.e., ^{144}Nd, E_α = 1.9, ^{146}Sm, E_α = 2.53, ^{148}Gd, E_α = 3.18 MeV). The bound-state in the final channel is unbound and extends much further out of the nucleus, than the two-proton wave function. The same observation holds for the projectile, ^{16}O, where the binding energies are -7.16 MeV for the α-particle and -22 MeV for the two-protons. The overlap of the four-particle wave functions thus extends to larger distances.

From expression (11) we deduce that an increase in R_o of 5% corresponding to 0.08 fm leads to a decrease of E_f and an increase of $Q_{opt\ 2}$ by 2.5 MeV. This is approximately the difference between Q_{opt}, ^{14}C and Q_{opt}, ^{12}C observed and shown in fig. 2.

This explanation of the difference in optimum Q-value for (^{16}O,^{14}C) and (^{16}O,^{12}C) reactions is consistent with the observation in earlier work (refs. [1,2,17]) that the grazing angle for the (^{16}O,^{12}C) reaction is consistently smaller compared to (^{16}O,^{15}N) and (^{16}O,^{14}C) reactions. The radius parameters r_o needed to describe the angular distributions were larger for the (^{16}O,^{12}C) compared to (^{16}O,^{15}N) and (^{16}O,^{14}C), (ref. [17])).

The presently measured ^{12}C spectra show some significant structures, which will be due to single states or groups of states in the final nucleus (see figs. 1, 3, 4, and 5). The level density being rather large at 6 to 8 MeV excitation in the relevant nuclei, one may conclude that a selective population of states occurs in the (^{16}O,^{12}C) reactions on these nuclei. Spectra with higher resolution are, however, necessary for a reasonable discussion of the nature of the observed selectivity.

5. Summary

The observed reactions clearly exhibit the features of direct transfer reactions. The strong Q-value dependence has been discussed. It is found that the position of the Q-value window can be satisfactorily described by a simple specification of the situation in the final channel if the angle of observation is larger than the grazing angle $\theta > \theta_o$; i.e., by interaction radius, R_o, charge product, Z_3Z_4, and scattering angle θ. Relation (1) in section 3.1 then defines E^f_{cm} and the position of the optimum Q-value is given by expression (11), which does not contain any information on the incident channel (except E^i_{cm}) nor on angular momentum transfer. Thus, at energies above the Coulomb barrier in many cases the strong absorption is mainly responsible for the shape and position of the Q-value window. Differences in Q_{opt} are attributed in this description to differences in interaction radii R_o. The differences in the interaction radii R_o (parameter r_o) then should be reflected in corresponding differences in the grazing angle θ_o, illustrating the close relation between the existence of a Q-value window and a "window" as a function of scattering angle (the cross sections peak at the grazing angle).

The two-proton transfer reactions induced by ^{16}O on the targets with the N = 82 closed neutron shell show clear effects due to the proton pairing interaction. The semiclassical properties of the reactions studied made a discussion of the enhancement factors in the two-proton transfer particularly easy and transparent, because the scattering process can be discussed independently. Total transfer probabilities, defined by semiclassical expressions have been derived from the data for the proton transfer, two-proton and "α-particle" transfer. Enhancement factors of 20-30 have been obtained for the $(^{16}O,^{14}C)$ ground state transitions. It

can be anticipated that the proton pairing interaction has its effects also on the "α-particle" transfer. Better resolution may be necessary to solve this question.

Distinctive regularities have been observed for the total transfer probabilities within the Q-value window to final states in different final nuclei. Whereas these regularities are easy to understand for the single-nucleon transfer reactions in the present nuclei (the spectra barely change from nucleus to nucleus) the understanding of the systematics for the multinucleon transfer displayed in fig. 9 needs further work.

Acknowledgments

The authors are indebted to Mr. A. Gamp and M. Feil for their help during the experiments. Discussions with Mr. F. Becchetti and E. Flynn are gratefully acknowledged. One of the authors (W.v.Oe) expresses his gratitude for the kind hospitality at the LBL.

References

1) H. Farraggi, J. Phys. Suppl. No. 11-12 (1971) C6-25, and references therein

2) G. C. Morrison, J. Phys. Suppl. No. 11-12 (1971) C6-25

3) D. G. Kovar, F. D. Becchetti, B. G. Harvey, F. Pühlhofer, J. Mahoney, D. W. Miller, and M. Zisman, Phys. Rev. Letters 29 (1972) 1023

4) P. R. Christensen, V. I. Manko, F. D. Becchetti, and R. J. Nickles, submitted to Nucl. Phys. (preprint)

5) P. J. A. Buttle and L. J. B. Goldfarb, Nucl. Phys. A176 (1971) 299, and references therein

6) R. A. Broglia and A. Winther, Nucl. Phys. A182 (1972) 112

7) W. von Oertzen, J. Phys. Suppl. No. 11-12 (1971) C6-233

8) M. Nagarajan, Nucl. Phys. A196 (1972) 34

9) T. Kammuri and H. Yoshida, Nucl. Phys. A129 (1969) 625

10) R. M. DeVries, Nucl. Phys. A178 (1972) 424, and to be published

11) a) H. Bohn, G. Daniel, M. R. Maier, P. Kienle, J. G. Cramer, and D. Proctel, Phys. Rev. Letters 29 (1972) 1337; b) J. P. Schiffer, H. J. Körner, R. Siemssen et al., ANL preprint (1973)

12) W. von Oertzen, N. Marquardt, and I. Inone, Proceedings of European Conference on Nuclear Physics, Vol. II, 53 (1972)

13) K. Alder, R. Morf, M. Pauli, and D. Trautmann, Nucl. Phys. A191 (1972) 399, and references therein

14) Code DWUCK by P. D. Kunz

15) B. H. Wildenthal, E. Newman, and R. L. Auble, Phys. Rev. C3 (1971) 1199

16) W. P. Jones, L. W. Borgman, K. T. Heoht, J. Bardwick, and W. C. Parkinson, Phys. Rev. C4 (1971) 580

17) A. Cunsolo, H. Farraggi, M. C. Lemaire, J. M. Loiseaux, M. C. Mermaz, A. Papineau, and J. L. Quebert, J. Phys. Suppl. No. 11-12, 32 (1971) C6-171

18) R. A. Broglia, C. Riedel, and T. Udagawa, Nucl. Phys. A184 (1972) 23, and, for example, Symposium on two-particle transfer, Argonne (1971) ANL

Table 1. Ground state Q-values Q_o, optimum Q-values Q_{opt1} (expression (8)) and Q_{opt2} (expression (11)), interaction distances R_o (r_o = 1.68 fm) and minimum distances in the classical orbit of the initial channel DI(θ_L = 150°) for ^{16}O induced reactions (a value of r_o = 1.63 fm gives $Q_{opt2} = Q_{opt}$ experimental for ^{14}C).

Target Nucleus	E_{in} [MeV]	Q_{opt1} [MeV] ^{15}N	^{14}C	^{12}C	Q_{opt2} [MeV] ^{15}N	^{14}C	^{12}C	DI[fm]	Reaction product	Q_o[MeV]
^{140}Ce	63	-6.2	-12.67	-12.67	-9.7	-15.5	-15.0	11.97	^{15}N	-6.9
R_o	64	-6.3	-12.87	-12.87	-10.65	-16.4	-15.9	11.78	^{14}C	-9.87
= 13.0 [fm]	65	-6.41	-13.07	-13.07	-11.54	-17.3	-16.77	11.60	^{13}C	-11.95
									^{12}C	-9.06
^{142}Nd	63	-6.25	-12.74	-12.74	-8.4	-14.4	-13.8	12.37	^{15}N	-7.94
R_o	64	-6.35	-12.94	-12.94	-9.3	-15.3	-14.7	12.17	^{14}C	-11.78
= 13.03 [fm]	65	-6.45	-13.14	-13.14	-10.2	-16.16	-15.6	11.99	^{13}C	-13.2
									^{12}C	-9.7
^{144}Sm	64	-6.38	-13.0	-13.0	-7.9	-14.1	-13.5	12.56	^{15}N	-8.9
R_o	65	-6.64	-13.2	-13.2	-8.8	-15.0	-14.4	12.37	^{14}C	-13.65
= 13.04 [fm]	66.5	-6.64	-13.5	-13.5	-10.2	-16.3	-15.80	11.95	^{13}C	-14.5
									^{12}C	-10.4

Table 2. Cross sections and transfer probabilities P_{tr} for (^{16}O,^{14}C) reactions to the ground states of final nuclei; errors are given with the cross sections only.

Target Nucleus	[MeV] E_L	θ_L	[fm] d_o	$d\sigma/d\Omega$[μb/sr]	σ_{tr}/σ_{EL}	[fm] ΔD	Correction factors F_1(DWBA)	F_2(SC)	$P_{tr}(d_o)$
^{140}Ce	63	150°	1.52	52±5	$8.8\cdot10^{-4}$	-.72	3.2	3.5	$2.8\cdot10^{-3}$
^{140}Ce	64	150°	1.50	21±5	$5\cdot10^{-4}$	-.74	4.2	4.0	$2.1\cdot10^{-3}$
^{142}Nd	63	150°	1.59	121±9	$1.54\cdot10^{-3}$	-.263	1.4	1.3	$2.2\cdot10^{-3}$
^{142}Nd	64	150°	1.56	197±12	$2.6\cdot10^{-3}$	-.308	1.4	1.35	$3.7\cdot10^{-3}$
^{142}Nd	65	150°	1.54	155±20	$2.6\cdot10^{-3}$	-.349	1.4	(1.5)	$3.7\cdot10^{-3}$
^{142}Nd	64	165°	1.54	110±17	$2.0\cdot10^{-3}$	-.305	2.0	1.35	$4.0\cdot10^{-3}$
^{142}Nd	65	165°	1.525	170±50	$4.5\cdot10^{-3}$	-.35	(1.2)	1.45	$4.5\cdot10^{-3}$
^{144}Sm	65	150°	1.7	50±9	$5.5\cdot10^{-4}$	.123	(2.5)	1.0	$(1.4\cdot10^{-3})$
^{144}Sm	66.5	154°	1.57	183±25	$3.66\cdot10^{-3}$	.037	1.0	1.05	$3.66\cdot10^{-3}$
^{144}Sm	66.5	170°	1.55	260±20	$1.0\cdot10^{-3}$	.037	1.0	1.05	$4.0\cdot10^{-3}$

Figure Captions

Fig. 1. Spectra of ^{15}N, ^{14}C, and ^{12}C nuclei emitted at backward angles in reactions induced by ^{16}O on ^{140}Ce, ^{142}Nd, and ^{144}Sm.

Fig. 2. Spectra of ^{12}C and ^{14}C nuclei from reactions induced by ^{16}O on ^{140}Ce at 64 MeV (in logarithmic scale). The ^{14}C spectrum was shifted by 5 channels.

Fig. 3. Spectra of ^{12}C and ^{14}C nuclei, same as in fig. 2, from reactions induced by ^{16}O on ^{140}Ce at 64 MeV.

Fig. 4. Spectra of ^{12}C and ^{14}C nuclei from reactions induced by ^{16}O on ^{142}Nd.

Fig. 5. a) ^{12}C spectra from reactions induced by ^{16}O on ^{142}Nd at three energies 63 MeV, 64 MeV, and 65 MeV. b) ^{15}N spectra as in fig. 5a.

Fig. 6. Angular distribution of total yield (divided by elastic yield) of ^{15}N, ^{14}C, and ^{12}C nuclei in reactions induced by ^{16}O on ^{140}Ce at 64 MeV.

Fig. 7. DWBA calculations for the dependence of the differential cross section at 150° for the two-proton transfer reaction $^{140}Ce(^{16}O,^{14}C)^{142}Nd$.

Fig. 8. Spectra of ^{14}C and ^{12}C nuclei (compare fig. 3) and DWBA calculations for the shape of the Q-value dependence of the cross section.

Fig. 9. Yield curves for ^{15}N, ^{14}C, and ^{12}C nuclei (integrated over the total energy spectrum) for reactions induced by ^{16}O on ^{140}Ce, ^{142}Nd, and ^{144}Sm. The energy above Coulomb barrier is scaled down by -6 MeV because deviations from Rutherford scattering are observed 10% below barrier.

Fig. 10. Ratios of the elastic scattering cross sections of ^{16}O and ^{14}C to the Rutherford scattering cross sections for the reactions shown in fig. 9. The Q-values indicate ground state Q-values in the $(^{16}O,^{14}C)$ reactions.

Fig. 11. Spectra of ^{15}N nuclei from proton transfer induced by ^{16}O on ^{140}Ce, ^{142}Nd, ^{144}Sm. For each spectrum the spectroscopic factors as determined from $(^{3}He,d)$ reactions (refs. [11,12]) are shown.

Fig. 12. Transition probabilities P_{tr} as function of parameter d_o, the minimum distance between ^{16}O and target. The points for ^{54}Fe, ^{64}Ni, and ^{88}Sr are derived from data in ref. [4]).

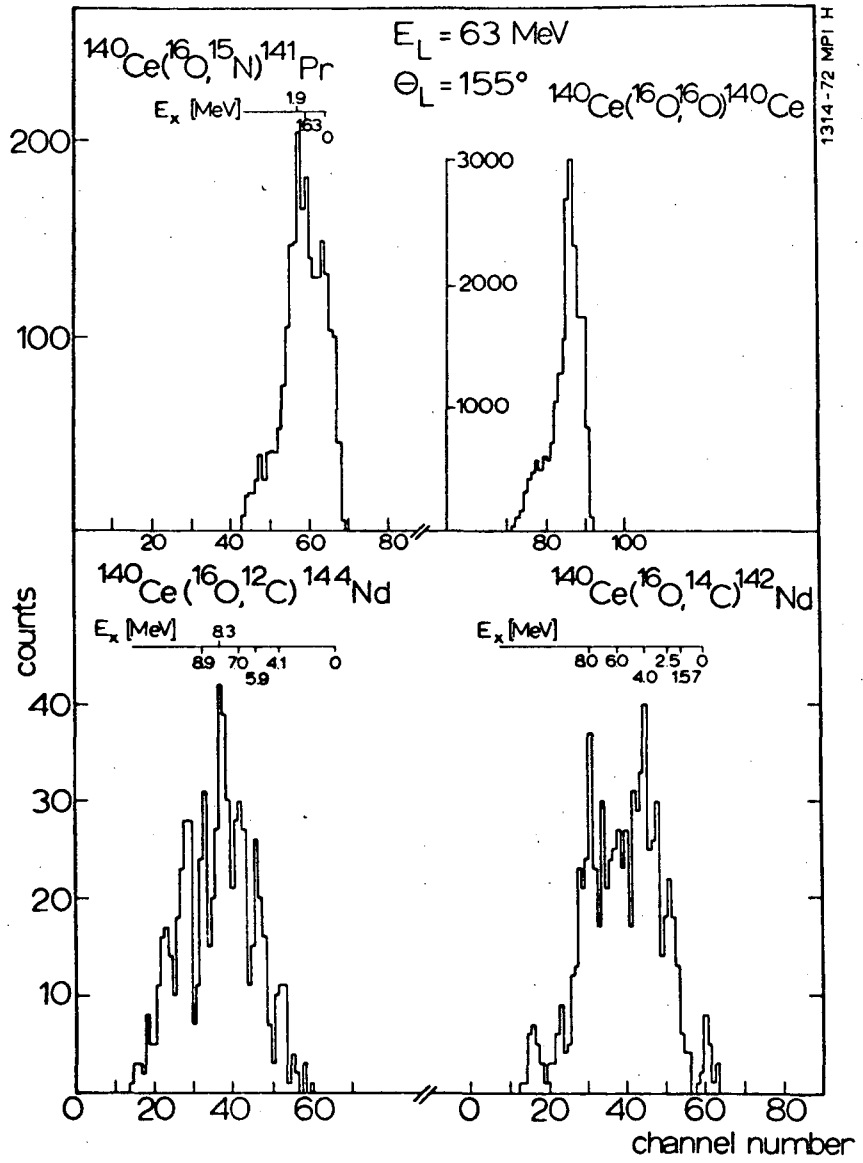
$^{140}Ce(^{16}O,^{15}N)^{141}Pr$
$E_L = 63$ MeV
$\Theta_L = 155°$
$^{140}Ce(^{16}O,^{16}O)^{140}Ce$
1314-72 MPI H
E_x [MeV] 1.9 1.63 0
$^{140}Ce(^{16}O,^{12}C)^{144}Nd$
E_x [MeV] 8.3 8.9 7.0 4.1 5.9 0
$^{140}Ce(^{16}O,^{14}C)^{142}Nd$
E_x [MeV] 8.0 6.0 2.5 4.0 1.57 0
counts
channel number

Fig. 1a

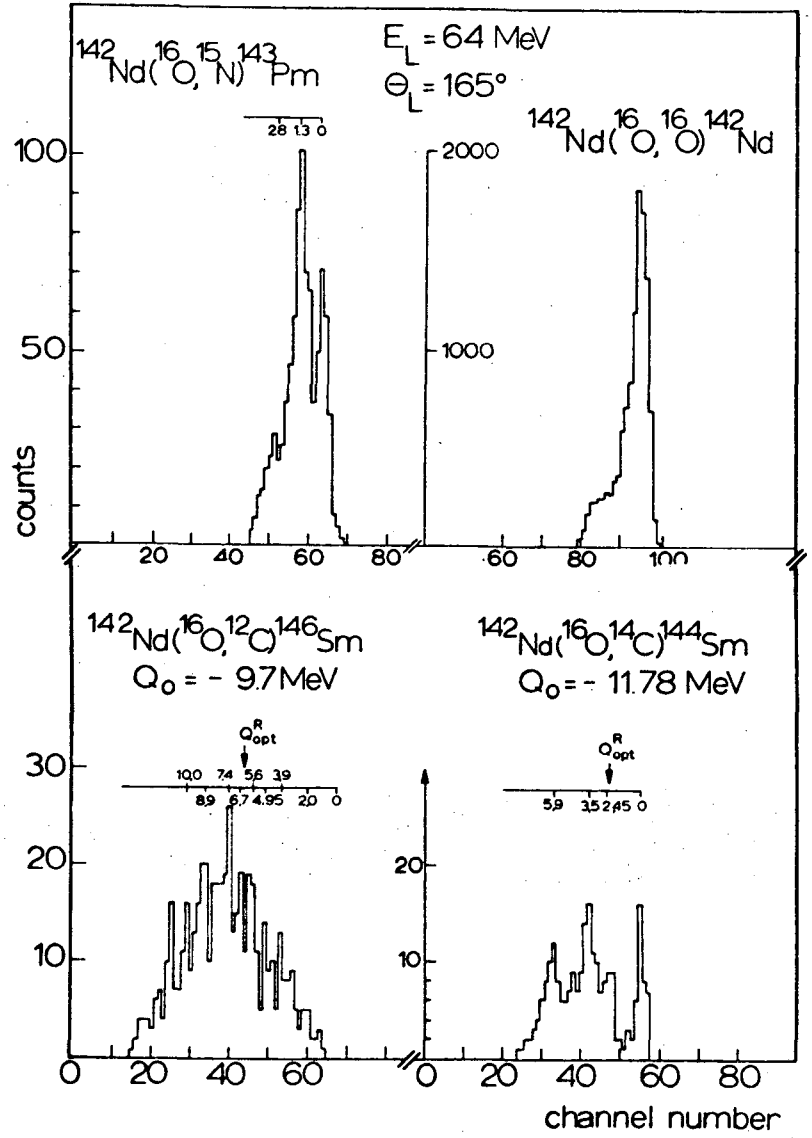
$^{142}Nd(^{16}O,^{15}N)^{143}Pm$
$E_L = 64$ MeV
$\Theta_L = 165°$
$^{142}Nd(^{16}O,^{16}O)^{142}Nd$
1315-72 MPI H
28 1.3 0
$^{142}Nd(^{16}O,^{12}C)^{146}Sm$
$Q_0 = -9.7$ MeV
Q^R_{opt}
10.0 7.4 5.6 3.9 8.9 6.7 4.95 2.0 0
$^{142}Nd(^{16}O,^{14}C)^{144}Sm$
$Q_0 = -11.78$ MeV
Q^R_{opt}
5.9 3.5 2.45 0
counts
channel number

Fig. 1b

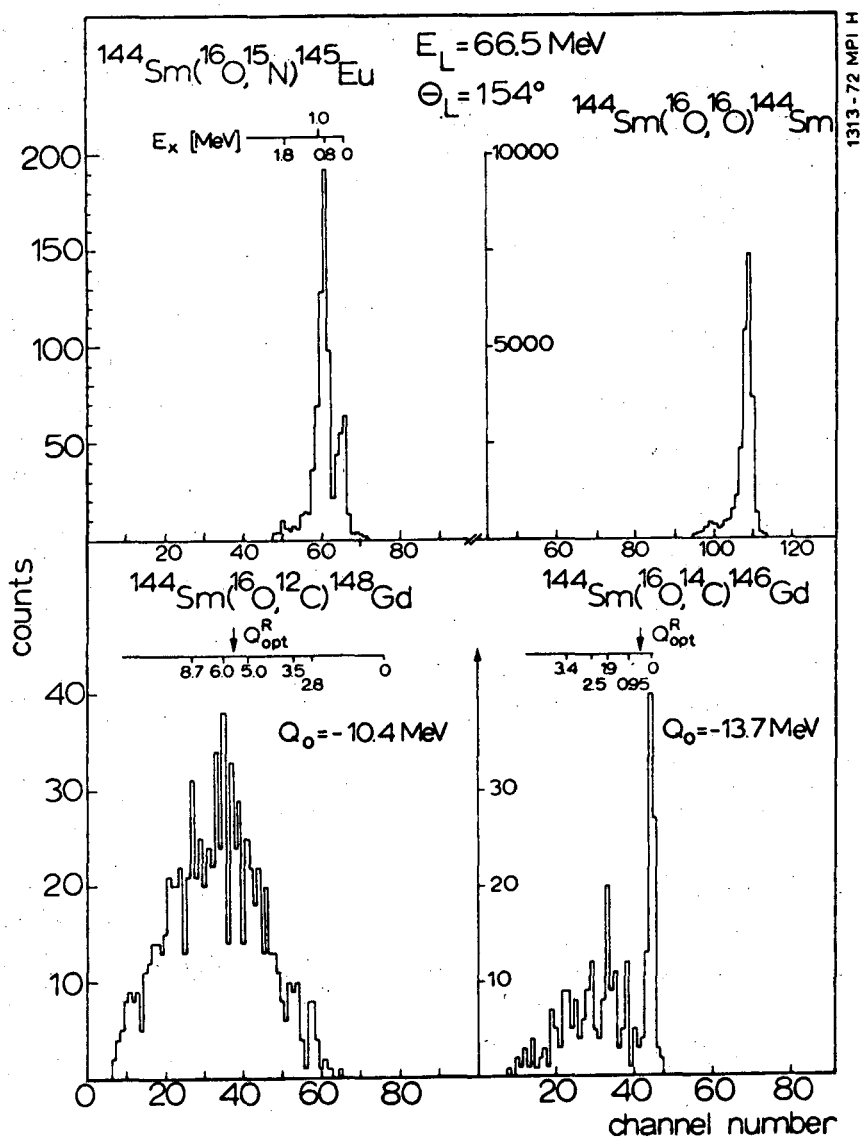
144Sm(16O,15N)145Eu
EL = 66.5 MeV
ΘL = 154°
144Sm(16O,16O)144Sm
Ex [MeV]
1.0
1.8
0.8
0
10000
5000
200
150
100
50
20
40
60
80
60
80
100
120
144Sm(16O,12C)148Gd
144Sm(16O,14C)146Gd
Q0 = -10.4 MeV
Q0 = -13.7 MeV
8.7
6.0
5.0
3.5
2.8
3.4
1.9
2.5
0.95
40
30
20
10
counts
0
20
40
60
80
channel number
1313-72 MPI H

Fig. 1c

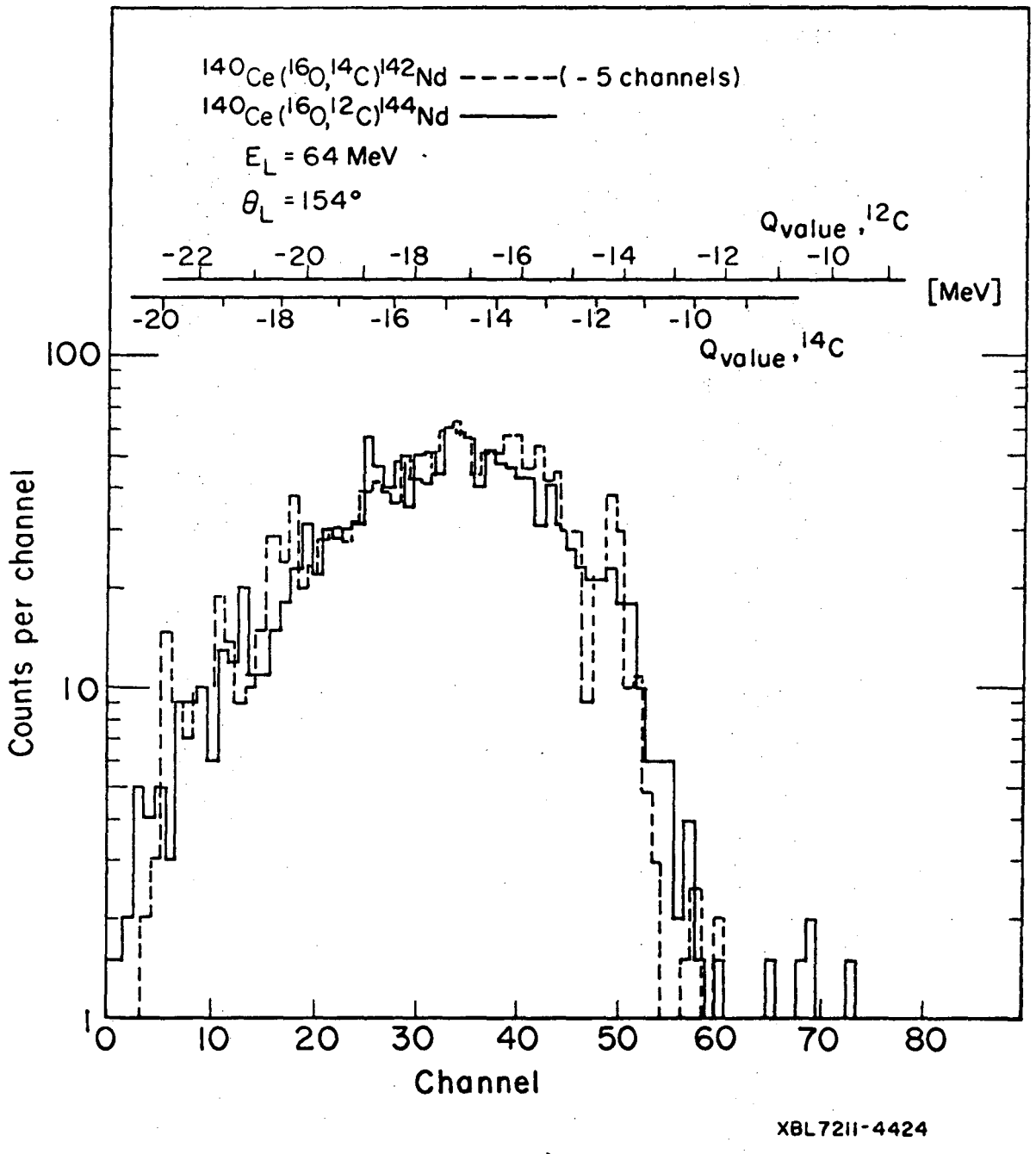
$^{140}Ce(^{16}O,^{14}C)^{142}Nd$ -----(- 5 channels)
$^{140}Ce(^{16}O,^{12}C)^{144}Nd$ ———
E_L = 64 MeV
θ_L = 154°
Q_{value}, ^{12}C
-22 -20 -18 -16 -14 -12 -10
[MeV]
-20 -18 -16 -14 -12 -10
Q_{value}, ^{14}C
100
10
1
Counts per channel
0 10 20 30 40 50 60 70 80
Channel
XBL7211-4424

Fig. 2

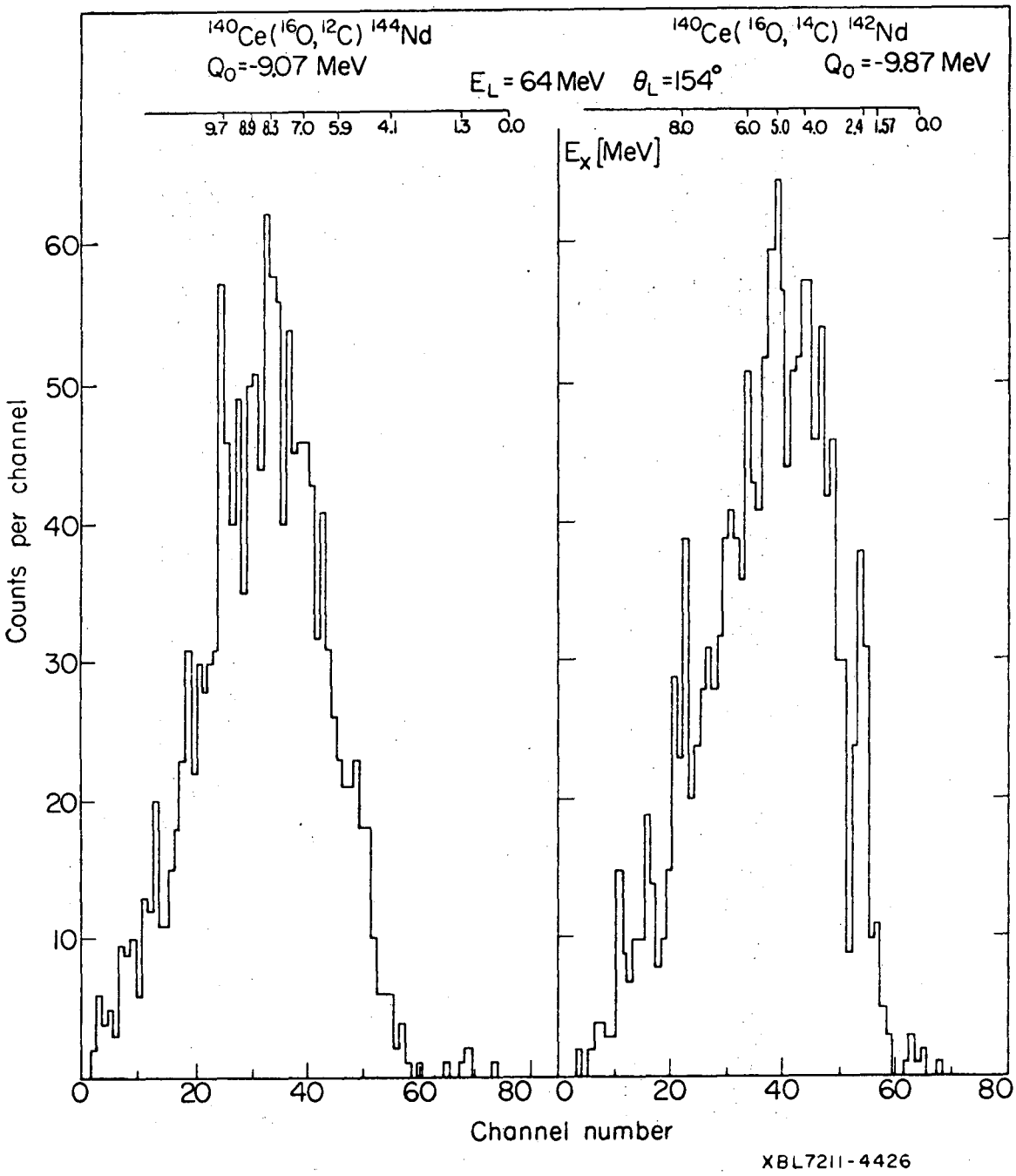
$^{140}Ce(^{16}O,^{12}C)\,^{144}Nd$
Q_0=-9.07 MeV
E_L = 64 MeV θ_L=154°
$^{140}Ce(^{16}O,^{14}C)\,^{142}Nd$
Q_0 = -9.87 MeV
9.7 8.9 8.3 7.0 5.9 4.1 1.3 0.0
8.0 6.0 5.0 4.0 2.4 1.57 0.0
E_x [MeV]
Counts per channel
Channel number
XBL7211-4426

Fig. 3

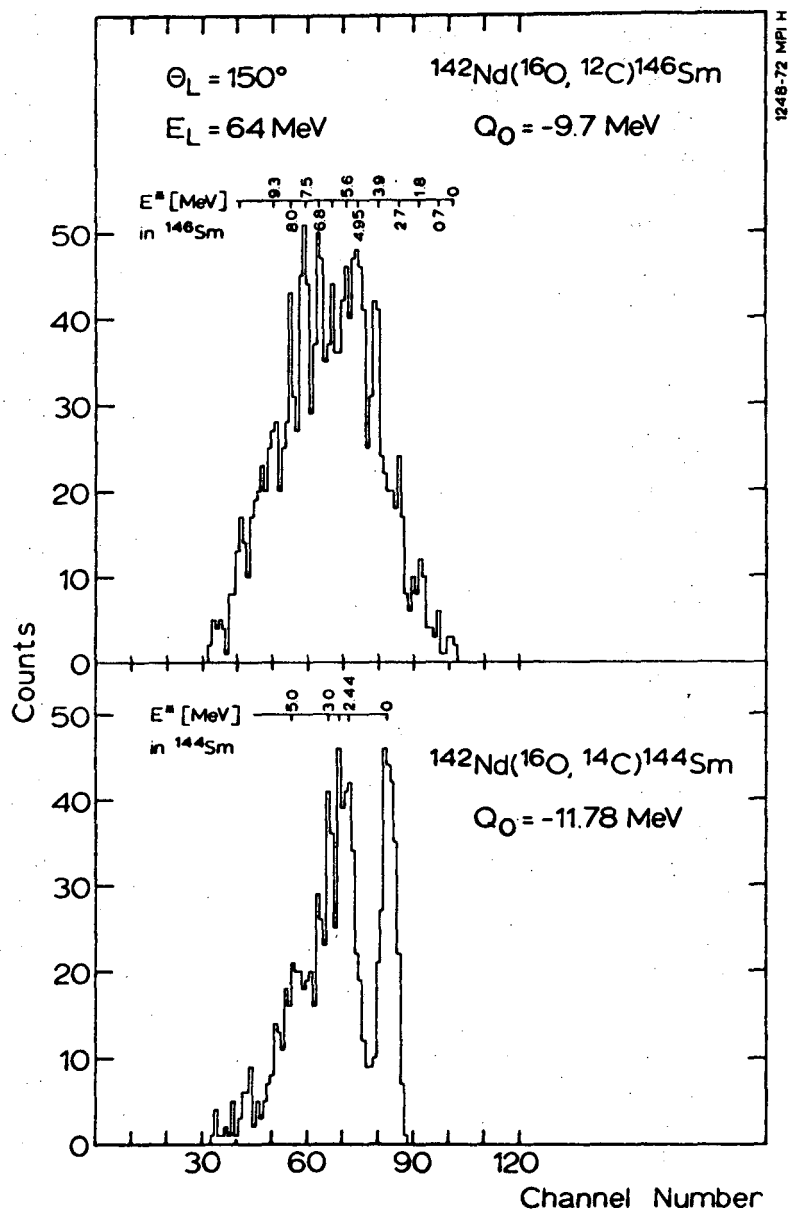
$\Theta_L = 150°$
$E_L = 64$ MeV
$^{142}Nd(^{16}O, ^{12}C)^{146}Sm$
$Q_0 = -9.7$ MeV
E^* [MeV] in ^{146}Sm
9.3
8.0
7.5
6.8
5.6
4.95
3.9
2.7
1.8
0.7
0
E^* [MeV] in ^{144}Sm
5.0
3.0
2.44
0
$^{142}Nd(^{16}O, ^{14}C)^{144}Sm$
$Q_0 = -11.78$ MeV
Counts
Channel Number
1248-72 MPI H

Fig. 4

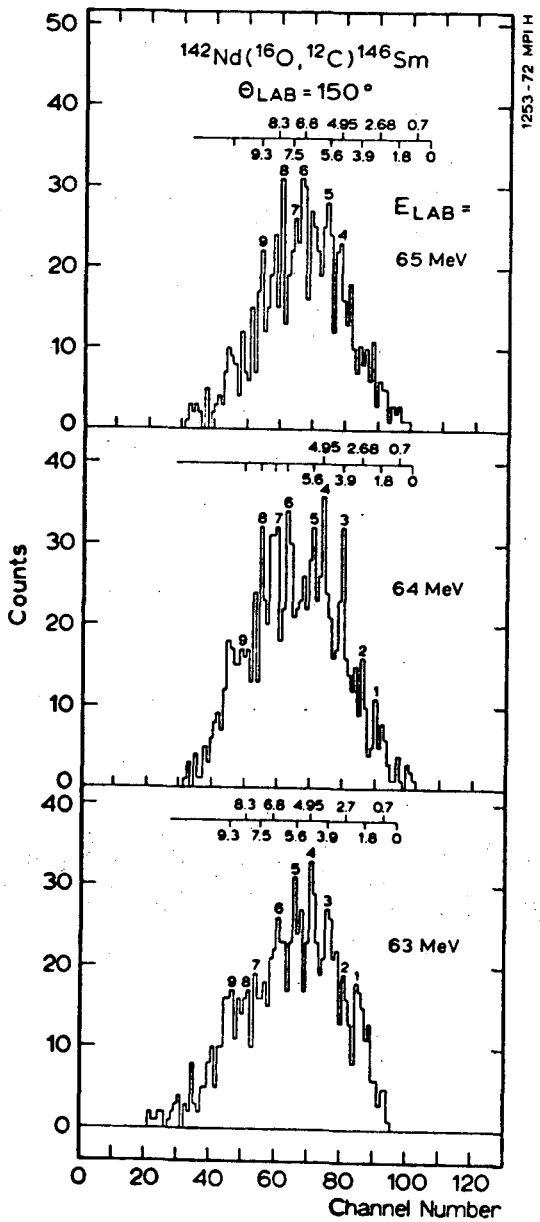
142Nd(16O, 12C)146Sm
ΘLAB = 150°
1253-72 MPI H
ELAB = 65 MeV
64 MeV
63 MeV
Counts
Channel Number

Fig. 5a

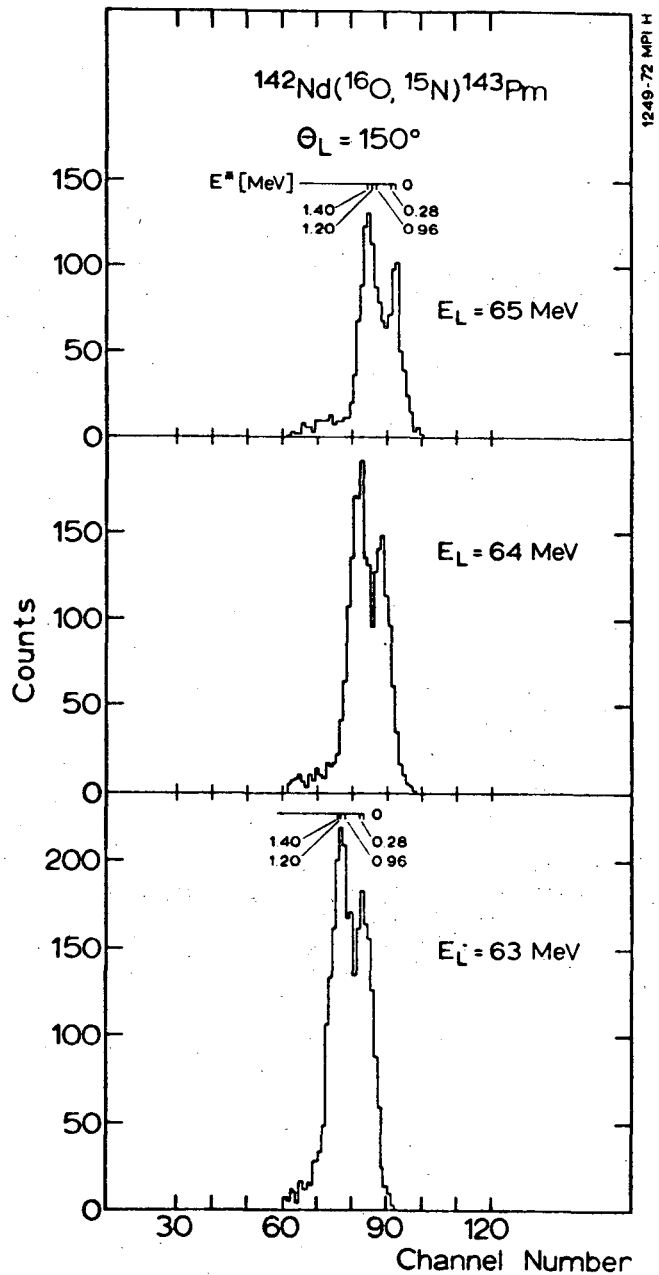
142Nd(16O, 15N)143Pm
ΘL = 150°
1249-72 MPI H
E* [MeV]
EL = 65 MeV
EL = 64 MeV
EL = 63 MeV
Counts
Channel Number

Fig. 5b

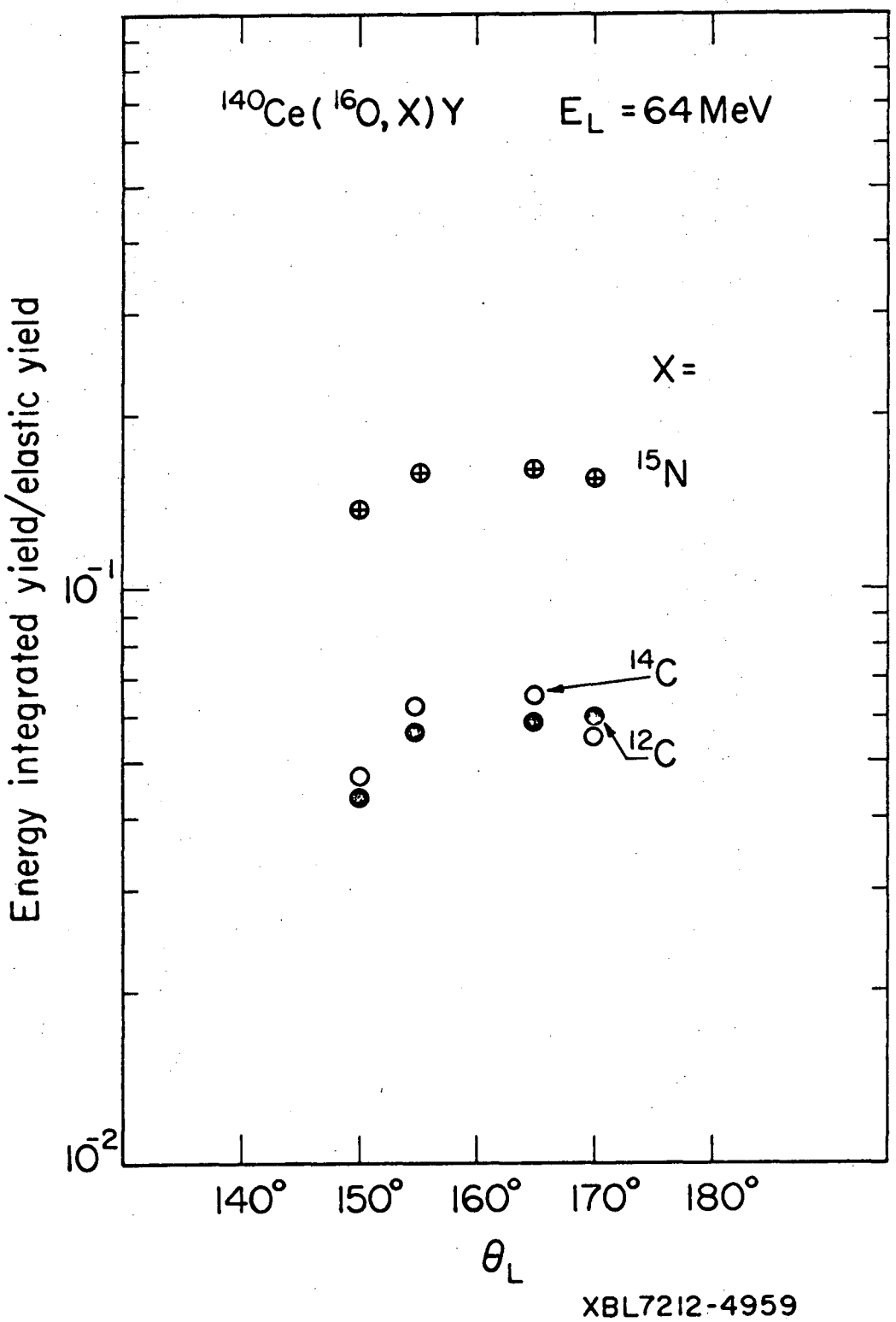
$^{140}Ce(^{16}O, X)Y$
$E_L = 64$ MeV
X =
^{15}N
^{14}C
^{12}C
Energy integrated yield/elastic yield
10^{-1}
10^{-2}
140°
150°
160°
170°
180°
θ_L
XBL7212-4959

Fig. 6

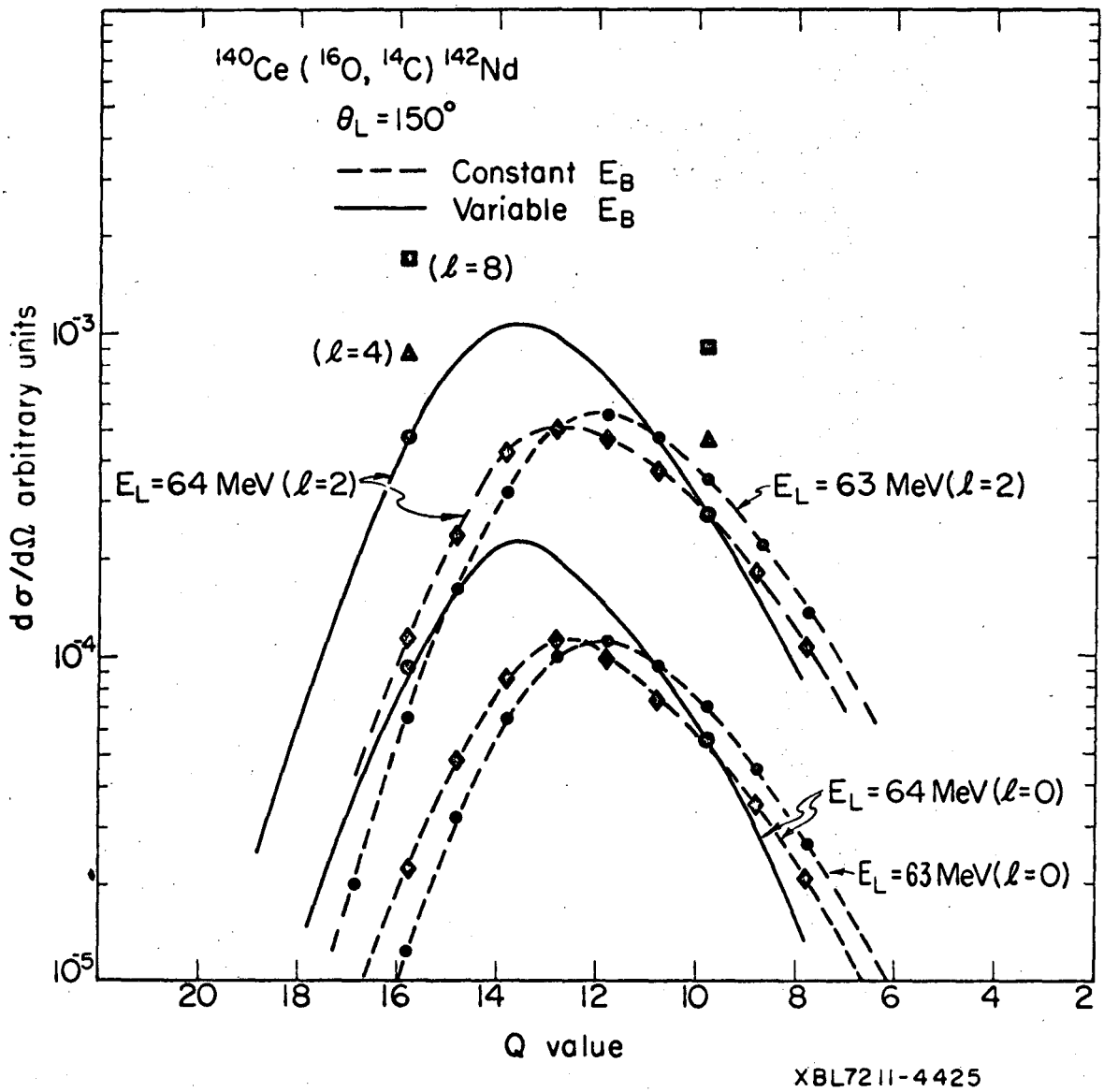
^{140}Ce (^{16}O, ^{14}C) ^{142}Nd
$\theta_L = 150°$
Constant E_B
Variable E_B
(ℓ=8)
(ℓ=4)
E_L=64 MeV (ℓ=2)
E_L = 63 MeV(ℓ=2)
E_L = 64 MeV (ℓ=0)
E_L = 63 MeV(ℓ=0)
dσ/dΩ arbitrary units
10^{-3}
10^{-4}
10^{-5}
20
18
16
14
12
10
8
6
4
2
Q value
XBL7211-4425

Fig. 7

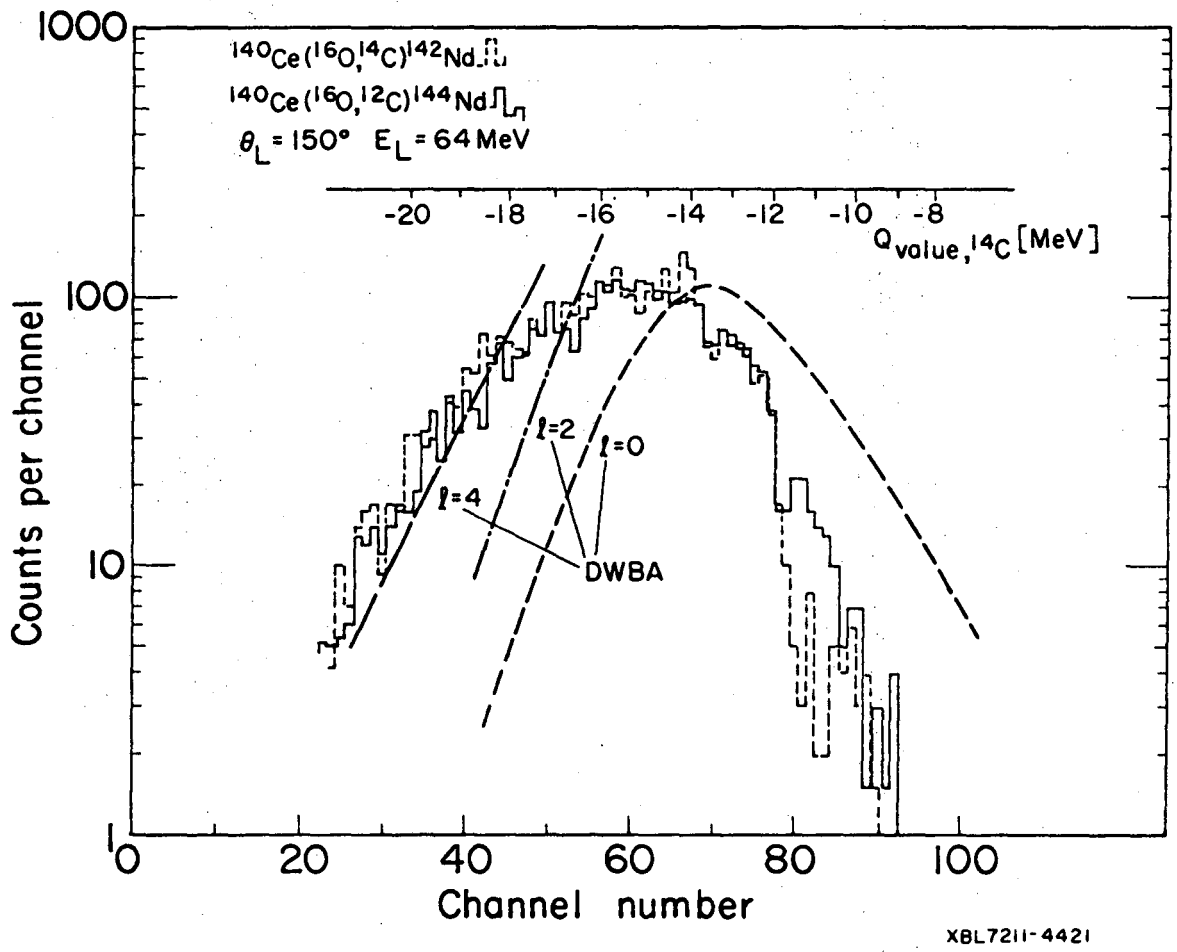
1000
100
10
1
Counts per channel
$^{140}Ce(^{16}O,^{14}C)^{142}Nd$
$^{140}Ce(^{16}O,^{12}C)^{144}Nd$
$\theta_L = 150°$ $E_L = 64$ MeV
-20 -18 -16 -14 -12 -10 -8
$Q_{value,^{14}C}$ [MeV]
$\ell=2$
$\ell=0$
$\ell=4$
DWBA
0 20 40 60 80 100
Channel number
XBL7211-4421

Fig. 8

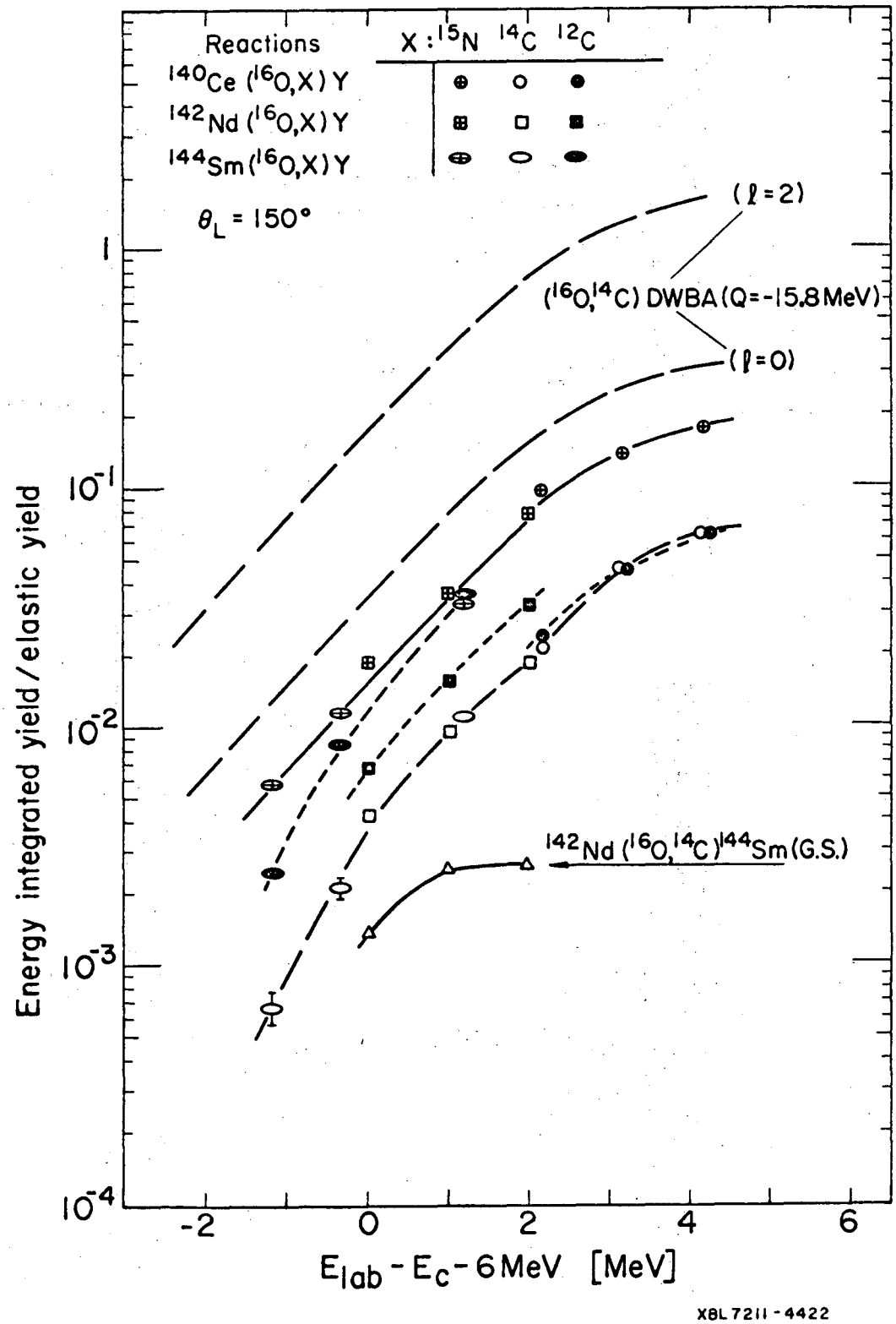
Reactions
X : 15N 14C 12C
140Ce (16O,X) Y
142Nd (16O,X) Y
144Sm (16O,X) Y
θL = 150°
(ℓ=2)
(16O,14C) DWBA (Q=-15.8 MeV)
(ℓ=0)
142Nd (16O,14C) 144Sm (G.S.)
Energy integrated yield / elastic yield
1
10-1
10-2
10-3
10-4
-2
0
2
4
6
Elab - Ec - 6 MeV [MeV]
XBL 7211-4422

Fig. 9

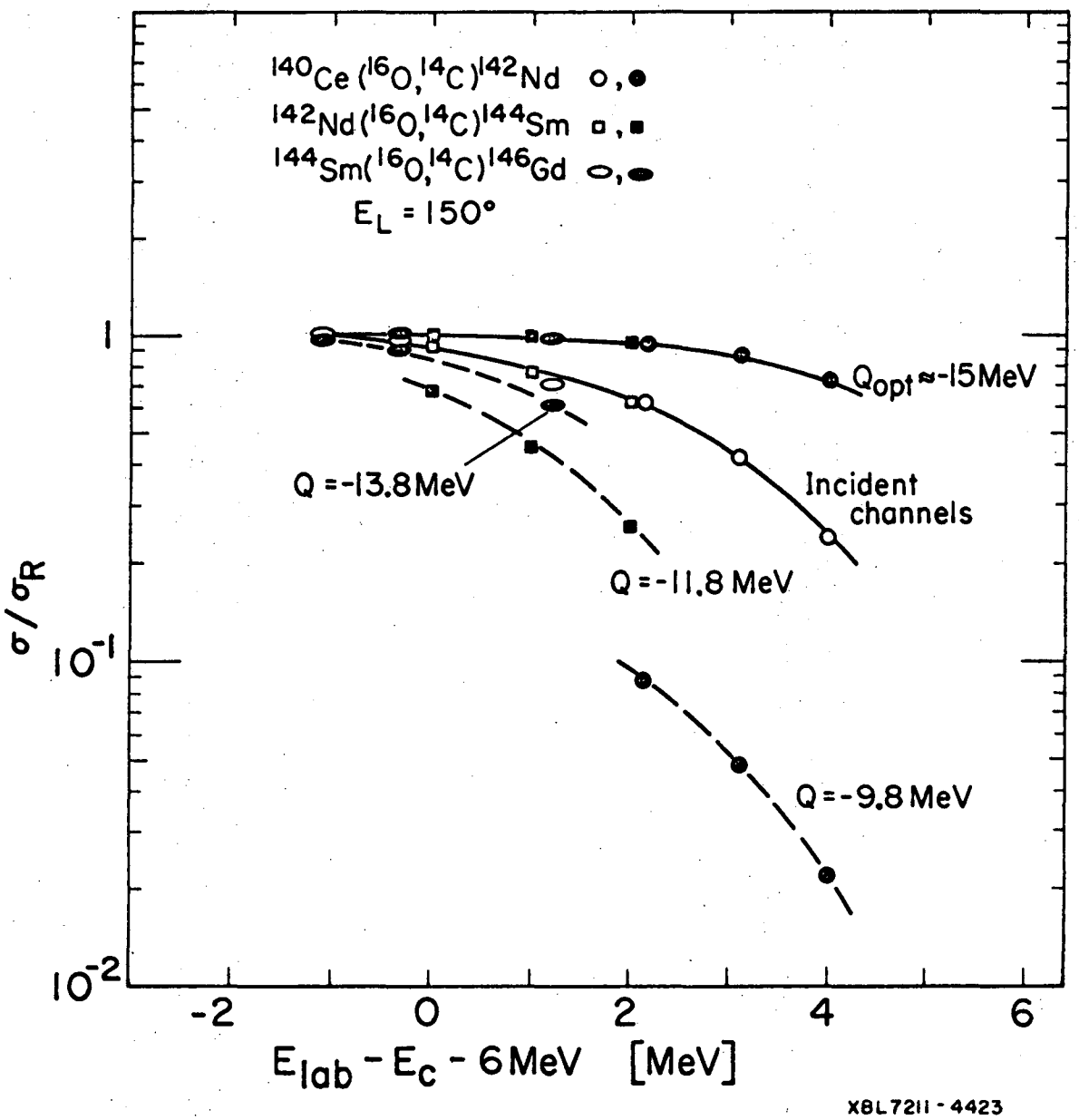
$^{140}Ce(^{16}O,^{14}C)^{142}Nd$ ○,●
$^{142}Nd(^{16}O,^{14}C)^{144}Sm$ □,■
$^{144}Sm(^{16}O,^{14}C)^{146}Gd$ ⬭,⬬
$E_L = 150°$
$Q_{opt} \approx -15$MeV
Incident channels
Q = -13.8MeV
Q = -11.8 MeV
Q = -9.8 MeV
σ/σ_R
1
10^{-1}
10^{-2}
-2
0
2
4
6
$E_{lab} - E_c - 6$MeV [MeV]
XBL7211-4423

Fig. 10

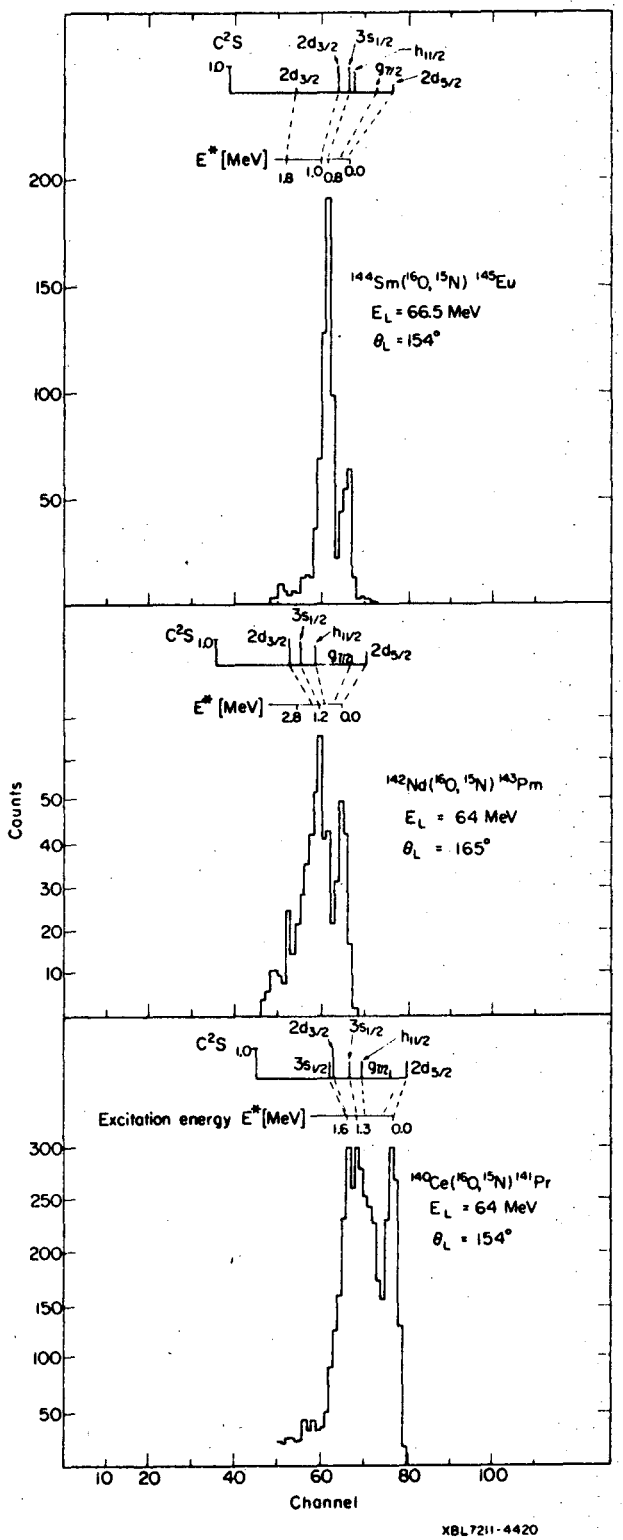
C²S
2d3/2
3s1/2
h11/2
g7/2
2d5/2
1.0
E* [MeV]
1.8 1.0 0.8 0.0
144Sm(16O, 15N) 145Eu
EL = 66.5 MeV
θL = 154°
2.8 1.2 0.0
142Nd(16O, 15N) 143Pm
EL = 64 MeV
θL = 165°
Excitation energy E* [MeV]
1.6 1.3 0.0
140Ce(16O, 15N) 141Pr
EL = 64 MeV
θL = 154°
Counts
Channel
XBL7211-4420

Fig. 11

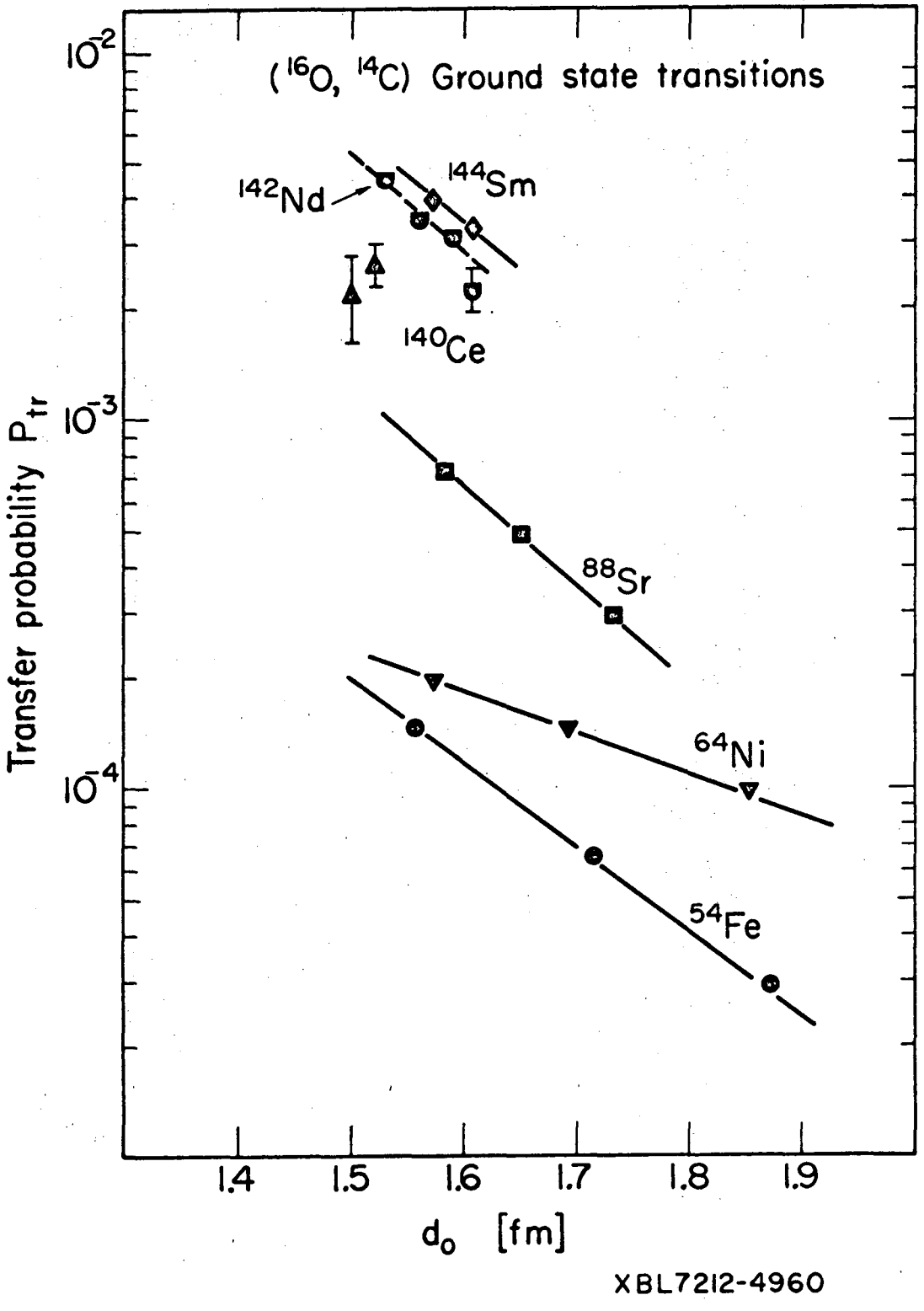
(^{16}O, ^{14}C) Ground state transitions
^{142}Nd
^{144}Sm
^{140}Ce
^{88}Sr
^{64}Ni
^{54}Fe
Transfer probability P_{tr}
10^{-2}
10^{-3}
10^{-4}
1.4
1.5
1.6
1.7
1.8
1.9
d_o [fm]
XBL7212-4960

Fig. 12

TECHNICAL INFORMATION DIVISION
LAWRENCE BERKELEY LABORATORY
UNIVERSITY OF CALIFORNIA
BERKELEY, CALIFORNIA 94720